ACS OMEGA

http://pubs.acs.org/journal/acsodf
Article

Host–Guest Dynamic Behavior of Melatonin Encapsulated in β-Cyclodextrin Nanosponges

Riccardo Ferrero, Stefano Pantaleone, Valentina Brunella, Marta Corno, Gonzalo Jiménez-Osés,* and Francesca Peccati*

Cite This: ACS Omega 2025, 10, 4660−4669
Read Online
ACCESS | Metrics & More | Article Recommendations | Supporting Information

ABSTRACT: Cyclodextrin-based nanosponges are cross-linked polymeric porous nanomaterials obtained by condensation of cyclodextrins with a polyfunctional reagent (cross-linker). Owing to their high surface area, they are attractive for encapsulation applications aimed at increasing the stability, solubility, and bioavailability of drugs. Due to the structural complexity of these emerging materials, computer modeling can provide atomistic-level insights into both the flexibility of nanosponges and their interactions with encapsulated drugs. In this contribution, we focus on nanosponges of β-cyclodextrin cross-linked with citric acid and provide full-atom models for linear and cyclic topologies. We use extensive molecular dynamics (MD) simulations to analyze the flexibility of these constructs and their interactions with encapsulated melatonin, a neurohormone involved in sleep-wake cycle regulation also used as an antioxidant and immunomodulator. We characterize the main interactions responsible for melatonin binding and show that it benefits from multivalence and crowding effects.

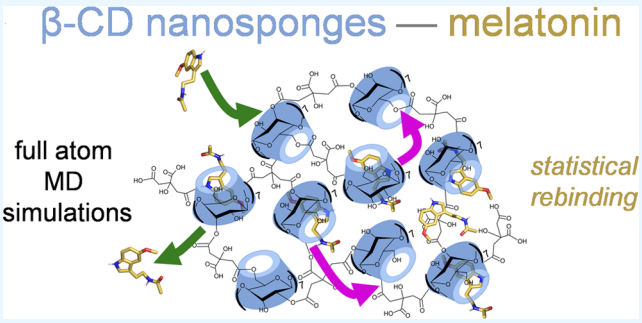

INTRODUCTION

Host–guest motifs are central to supramolecular chemistry; they involve the formation of complexes resulting from the preferential association of a guest molecule with a host.[1,2] A pharmaceutical application of host–guest chemistry is drug delivery, where the formation of a complex in which the guest is a pharmacologically active compound can have several beneficial effects on its physical and pharmacokinetic properties.[3,4] Hosts are often macrocycles that enhance the solubility and formulation stability of various hydrophobic drugs, increase cell permeability for charged species, and occasionally reduce toxicity.[2]

Among them, cyclodextrins (CDs) have received attention as inexpensive, nontoxic, biocompatible and biodegradable compounds.[5] CDs are cyclic oligosaccharides composed of α-D-glucopyranose units linked by α-1,4 glycosidic bonds. They are classified according to the number of glucopyranose units (α-CD, β-CD, and γ-CD contain six, seven, and eight units, respectively). CDs have a truncated cone structure with an inner hydrophobic region dominated by the glucopyranose CH groups capable of binding small hydrophobic molecules, and an outer region rich in hydroxyl groups that confer moderate solubility.[4] CDs have intrinsic torsional flexibility around the glycosidic bonds, which enables dynamic rearrangement and allows them to encapsulate various guests through induced fit.[6−9]

β-CD is known to bind melatonin (MT), a natural neurohormone involved in regulating the sleep-wake cycle. It is used to treat sleep disorders and has also demonstrated antioxidant properties, as well as involvement in regulating the immune system.[10,11] MT is a methoxyindole with poor water solubility, which can be enhanced by the formation of a 1:1 inclusion complex with β-CD.[12] Some of us have recently investigated β-CD and the MT:β-CD inclusion complex conformations with quantum mechanics methods identifying van der Waals interactions as the main driving force for complex formation.[13,14]

Nanosponges are nanoscale drug carriers with a three-dimensional structure formed by cross-linked polymers. Several classes of such materials have been proposed based on the nature of the polymer; among them, polyalcohol-based and carbohydrate-based nanosponges. These materials are attractive because they can encapsulate a wide range of drugs of varying sizes and shapes and these characteristics can be fine-tuned by controlling pore sizes and surface properties. As such, they allow control over drug uptake and release. Being

Received: October 14, 2024
Revised: January 4, 2025
Accepted: January 10, 2025
Published: January 28, 2025

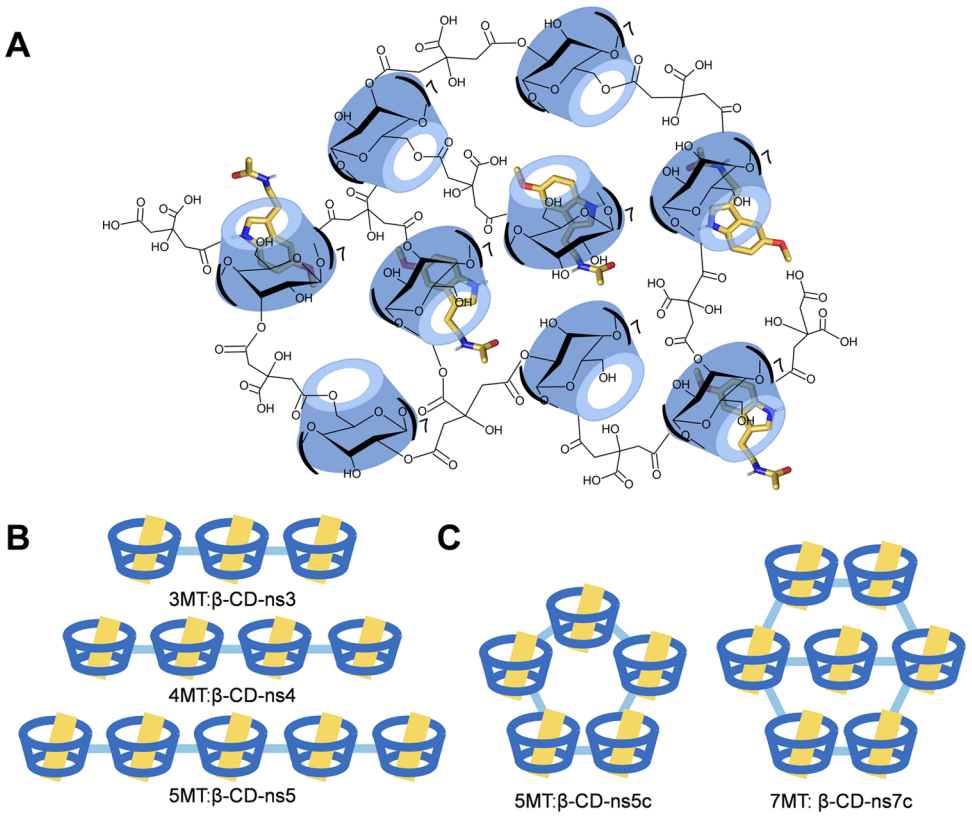

Figure 1. (A) Structure of β-CD nanosponges cross-linked with citric acid in complex with MT. β-CD units are shown as blue truncated cones and melatonin (MT) molecules as yellow sticks. (B) Acyclic nanosponge topologies considered in this work. (C) Cyclic nanosponge topologies considered in this work. β-CD units are shown as blue truncated cones, citric acid units as light blue lines, and MT molecules as yellow rectangles.

synthesized from biodegradable materials, they generally show low toxicity and have low manufacturing cost. Their high biocompatibility and tunability by using different rations of polymers and cross-linking agents makes them advantageous over other drug delivery systems such as protein-based, lipid-based, and metal nanoparticles.[15−18]

CD-based nanosponges are an emerging class of porous polymers in which cyclodextrins are cross-linked to form a three-dimensional network (Figure 1A). They can form complexes with a wide range of both lipophilic and hydrophilic molecules via both inclusion and noninclusion complexation. As monomeric CD, they are biocompatible and show high binding versatility due to the coexistence of lipophilic cavities (intra-CD) and hydrophilic channels (inter-CD). For these reasons, they find a variety of applications in the fields of drug delivery, diagnostics, cosmetics and environmental control.[9,19]

Despite the wide range of applications, the structure and properties of nanosponges are not fully characterized yet. Computational approaches based on molecular dynamics have provided precious insight into structural aspects (e.g., swelling behavior[20]), properties (e.g., aggregation[21]) and binding behavior (e.g., interaction modes[22]) of nanosponges.

Recently, a CD-based nanosponge has been synthesized in water using citric acid as the cross-linking agent, demonstrating the ability to bind and stabilize MT.[23−25] An outline of its structure is shown in Figure 1A. Nanosponge structures are varied at the molecular level owing to the high number of reactive hydroxyl groups in β-CD and carboxylic groups in citric acid.[15] This leads to high structural complexity that makes it challenging to characterize the interactions with guests in detail. In this work, we use microsecond molecular dynamics (MD) to model the interactions between β-CD-based guests of different complexity and MT. In particular, we present full-atom three-dimensional structures of β-CD units cross-linked with citric acid through α-glucose C6 and C2 hydroxyl groups, arranged in both acyclic and cyclic topologies, serving as minimal nanosponge models. These topologies are shown in Figures 1B and 1C, respectively. We compare MT stabilizing interactions in the nanosponge models with those in the monomeric inclusion complex to identify how flexibility and binding is affected by polymerization and molecular crowding.

METHODS

Conventional Molecular Dynamics Simulations. MD simulations were carried out with AMBER 22[26] using the GLYCAM-06j[27] force field for β-CD, gaff2[28] for citric acid and melatonin, and the OPC3,[29] OPC,[30] and TIP3P[31] force fields for water. β-CD nanosponges models were immersed in a water box with a 10 Å buffer of water molecules and neutralized by adding explicit Na^+ counterions (Li-Merz 12−6 normal usage set[32]). A two-stage geometry optimization approach was implemented. The first stage minimizes only the positions of solvent molecules and ions, and the second stage is an unrestrained minimization of all the atoms in the simulation cell. The systems were then heated by incrementing the temperature from 0 to 300 K under a constant pressure of 1 atm and periodic boundary conditions. Harmonic restraints of 10 kcal mol^{-1} $Å^{-2}$ were applied to the solute, and the Andersen temperature coupling scheme[33] was used to control and equalize the temperature. The time step was kept at 1 fs during the heating stage, allowing potential inhomogeneities to

https://doi.org/10.1021/acsomega.4c09367
ACS Omega 2025, 10, 4660−4669

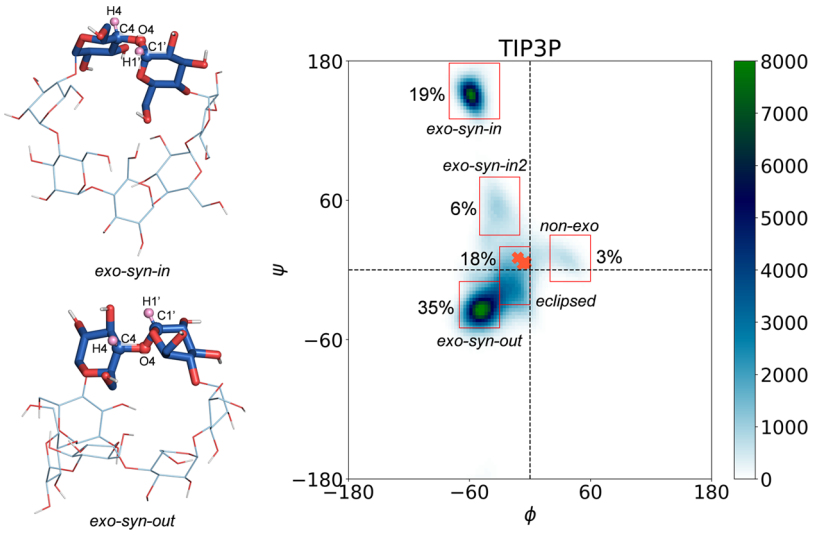

Figure 2. 2D histogram of β-CD ϕ and ψ angles along a 5 μs molecular dynamics simulation with TIP3P water. Angles definition: ϕ: H1′-C1′−O4-C4, ψ: C1′−O4−C4-H4. The color bar is a measure of bin population. Average ϕ and ψ values for the glycosidic bonds of β-CD in crystallographic structures from the Protein Data Bank (IDs 3CGT, 1DMB, 1BFM, and 1VFO) are shown as a red crosses. Glycosidic bond conformations corresponding to highly populated regions are shown as sticks with relevant atoms for ϕ and ψ definition shown as spheres. Nonpolar hydrogens are omitted for clarity.

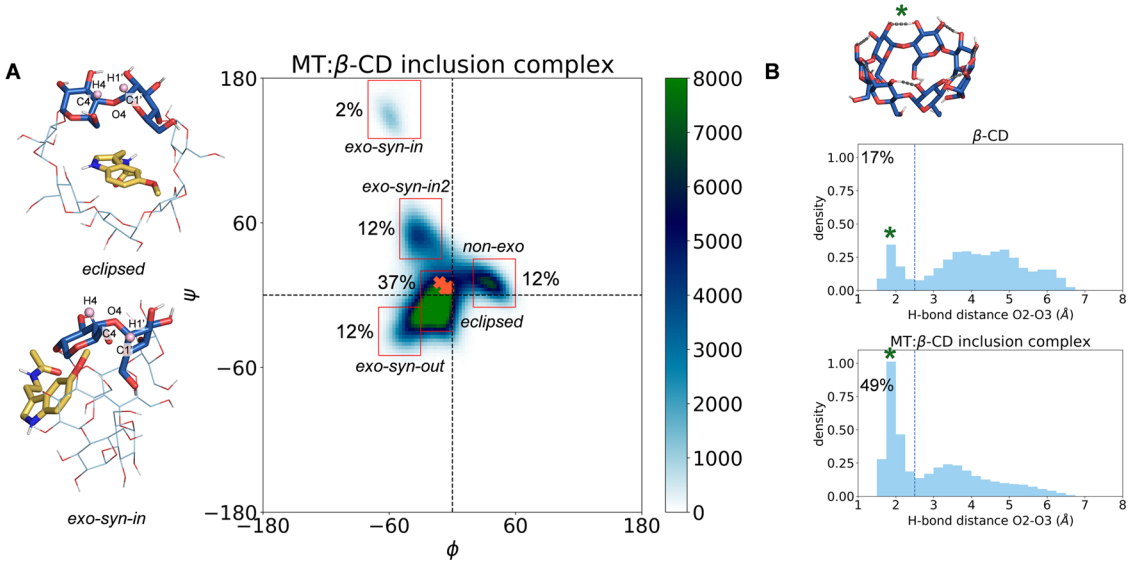

Figure 3. (A) 2D histogram of monomeric MT:β-CD inclusion complex ϕ and ψ angles along three 5 μs molecular dynamics simulations initiated from three different geometries (15 μs in total). Average ϕ and ψ values for the glycosidic bonds of β-CD in crystallographic structures from the Protein Data Bank (IDs 3CGT, 1DMB, 1BFM, and 1VFO) are shown as red crosses. Angles definition: ϕ: H1′-C1′−O4-C4, ψ: C1′−O4−C4-H4. The color bar is a measure of bin population. Selected glycosidic bonds conformations are shown as sticks with relevant atoms for ϕ and ψ definition shown as spheres. MT is shown as yellow sticks. Nonpolar hydrogens are omitted for clarity. (B) Distribution of hydrogen bond distances between the hydroxyl groups at positions 2 and 3 of neighboring glucose units in the MD simulations of free β-CD and the monomeric MT:β-CD inclusion complex with TIP3P water. A threshold distance of 2.5 Å is used to compute the percentage of hydroxyl groups engaging in hydrogen bonds.

self-adjust. Once equilibrated, the system was subjected to a 2 ns constant volume molecular dynamics simulation at 300 K using the SHAKE algorithm[34] and a 2 fs time step. Long-range electrostatic effects were modeled using the particle mesh Ewald method.[35] A cutoff of 8 Å was applied to Lennard-Jones interactions. Production was run as ten 500 ns replicas for monomeric β-CD, free MT, and the monomeric MT:β-CD inclusion complex (5 μs), and as four 500 ns replicas for the nanosponge models (2 μs). For MT:β-CD, we considered three different initial structures for a total simulation time of 15 μs. Molecular dynamics simulations for maltose capped with a methoxy group at the reducing end were run as ten 500 ns replicas (5 μs) with GLYCAM-06j and TIP3P water. Analysis was performed with *cpptraj*.[36]

Hamiltonian Replica Exchange Umbrella Sampling. Hamiltonian Replica Exchange Umbrella Sampling (REUS) simulations[37] were performed with AMBER 22[26] to estimate the β-CD−MT binding free energy. Systems were equilibrated using the same procedure described above for conventional MD simulations, with a 30 Å buffer of TIP3P water molecules.

https://doi.org/10.1021/acsomega.4c09367
ACS Omega 2025, 10, 4660−4669

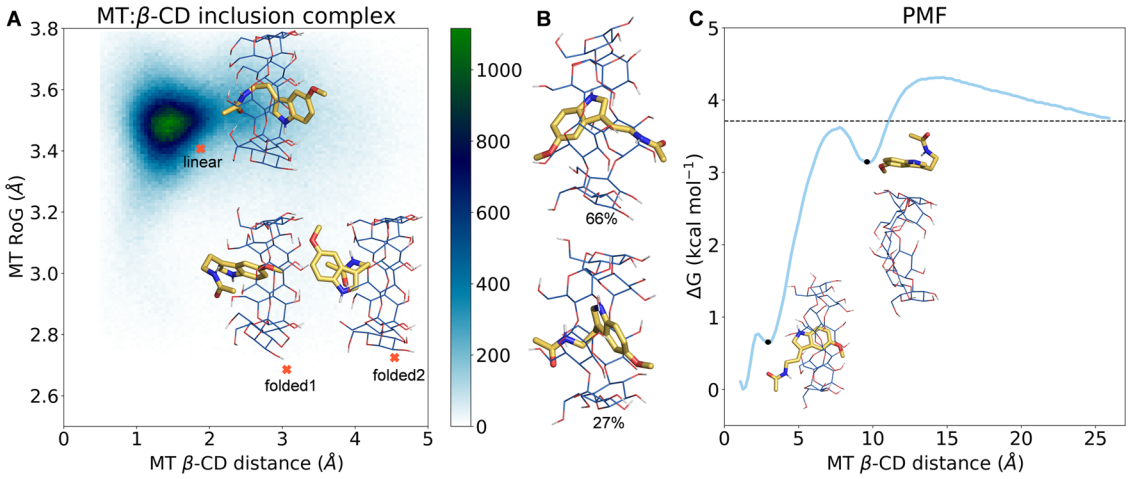

Figure 4. (A) 2D histogram of MT:β-CD inclusion complex geometric arrangements along three 5 μs molecular dynamics simulations initiated from three different geometries (15 μs in total). The x-axis is the distance between the center of mass of the glycosidic oxygens (O4) of β-CD and the center of mass of its bound MT in the initial geometry (heavy atoms). The y-axis is the radius of gyration of MT (heavy atoms). The three geometries used as the starting point for the MD simulations are shown and their positions on the plot marked with red crosses. (B) Representative structures of the most populated geometric clusters observed along the MD simulation of the MT:β-CD inclusion complex. The population of each cluster is shown as percentage of the simulation time. (C) Potential of mean force for MT unbinding from β-CD with representative geometries of higher energy local minima. β-CD is represented with blue lines and MT with yellow sticks; nonpolar hydrogens are omitted for clarity.

The unbinding coordinate was defined as the distance between the centers of mass of the glycosidic (O4) oxygens of β-CD and that of the MT molecule. Fifty windows were used with a 0.5 Å increase of the unbinding coordinate (from 1.3 to 25.8 Å) and a force constant of 5 kcal mol^{-1} Å^{-2}. Each window was run for a total of 50 ns, and the first 2 ns were discarded as equilibration, leaving a 48 ns sampling time. Molecular dynamics simulations were run at constant volume and at 300 K using the SHAKE[34] algorithm and a 2 fs time step, with a cutoff of 14 Å for Lennard-Jones interactions. The Langevin thermostat[38] was used with a collision frequency γ of 2.0 ps^{-1}. Distance values for each window were written every 100 steps (0.2 ps). Potentials of mean force were computed with the Weighted Histogram Analysis Method as implemented in the WHAM program.[39] The number of integration bins was set to 146 and the temperature to 300 K.

RESULTS AND DISCUSSION

Conformational Analysis of Monomeric β-CD in Solution. First, we performed extensive MD simulations of the monomeric β-CD in solution (5 μs) to analyze its conformational landscape in the absence of a guest using the GLYCAM-06j force field[27] for β-CD and three water force fields (OPC3,[29] OPC,[30] and TIP3P[31]). A symmetric, quantum mechanically optimized structure published elsewhere was used as the starting geometry.[13]

We characterized the flexibility of the system collectively by analyzing the distribution of the ϕ and ψ angles of the seven chemically equivalent glycosidic bonds (Figure 2). The distribution of ϕ and ψ values reveals multiple conformations around the glycosidic bonds. This is in stark contrast with the very rigid α-1,4 glycosidic bond in the simplest related disaccharide maltose (with a unique conformation at $\phi \sim -40°$ and $\psi \sim -30°$, see Figure S1) and in the many crystallographic structures available for β-CD which are restricted to a relatively small area of the ϕ,ψ space near 0°,0° (*eclipsed* conformation) driven by a network of cooperative hydrogen bonds between the hydroxyl groups at C2 and C3.[40] The two most populated bond conformations in β-CD are centered at $\phi = -49°$, $\psi = -35°$ (*exo-syn-out*) and at $\phi = -57°$, $\psi = 150°$ (*exo-syn-in*). Here the *out* and *in* labels refer to the orientation of the α-Glc hydroxymethyl group with respect to the center of the β-CD cavity: outward and inward, respectively. Sample frames from molecular dynamics corresponding to these conformations are shown in Figure 2. The remaining frames are distributed across three further clusters spanning over other *exo-syn* and *non-exo* conformations. These results are in line with previous computational and NMR studies[6−8] that highlight the flexible nature of CDs, which is deeply affected by solvent polarity,[41] and the need of a conformational ensemble to characterize their properties in solution. Analysis of glucose conformation through the puckering angles shows the expected behavior for α-glucose, with 95% of the rings in $^4C_1$ conformation (Figure S2).

Both global and individual glycosidic bond populations obtained with different water force fields are shown in Figure S1. Global populations are essentially identical, with deviations of only up to 2%. All three force fields also show equivalent distributions of individual glycosidic bond conformations revealing that no more than two of them can simultaneously be found in the *exo-syn-in* conformation, and that the seven bonds show equal flexibility. Therefore, as we did not observe any effect from the force field, we performed all subsequent simulations with TIP3P; as a 3-points water model, it is more computationally efficient than OPC (4-points) and has been extensively used and validated in combination with GLYCAM.[42−44]

Monomeric Inclusion Complex. Next, we performed MD simulations of the monomeric MT:β-CD inclusion complex to characterize its host−guest interactions. MD simulations were initialized from three different starting geometries, named *linear*, *folded1*, and *folded2* (*vide infra*, Figure 3). These structures, published elsewhere, feature a symmetric β-CD geometry with ϕ and ψ values of −7 and 7°, respectively, resembling the crystallographic *eclipsed* conformation and a variety of MT arrangements.[13,14,45] For each starting structure, we ran 5 μs MD simulations and analyzed the

https://doi.org/10.1021/acsomega.4c09367
ACS Omega 2025, 10, 4660−4669

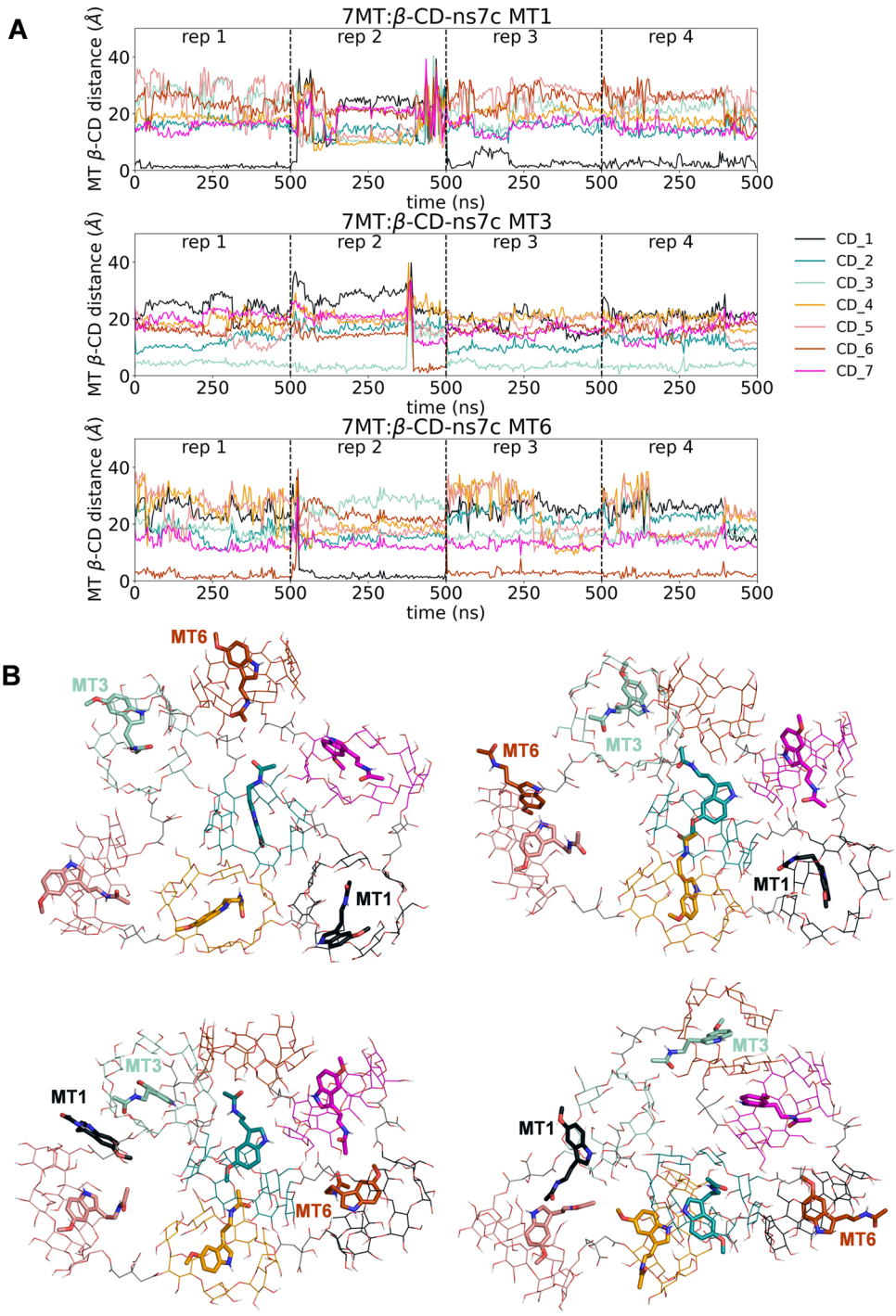

Figure 5. (A) Distribution of MT1, MT3 and MT6 distances from each of the seven β-CD units of the β-CD-ns7c nanosponge model along the four 500 ns MD replicas (rep 1 to 4). Distances are computed between the center of mass of the six glycosidic oxygens (O4) of each β-CD unit and the center of mass of MT computed using the heavy atoms. Each MT is color-coded according to the β-CD unit it is bound to in the initial geometry. (B) Selected frames from a single MD simulation (replica 2) illustrating MT's spontaneous unbinding and rebinding to a different β-CD. Color coding matches panel A. MT units are shown as sticks, nanosponges as lines, and nonpolar hydrogens are omitted for clarity.

combined 15 μs simulation collectively. Formation of the inclusion complex shifts the conformational preference around the glycosidic bonds depleting the *exo-syn-out* and *exo-syn-in* conformations in favor of the *eclipsed* one. A sample frame from the MD simulation of the inclusion complex is shown at the top of Figure 3A in which MT is inserted at the β-CD cavity with the cyclodextrin in an *eclipsed* conformation. Owing to the steric hindrance imposed by the inserted MT and the depletion of water, glycosidic bonds favor the *eclipsed* conformation when MT is fully bound. This is shown for a sample frame of the MD simulation at the bottom of Figure 3A, where the *exo-syn-in* conformation can be attained only upon partial MT unbinding. In the *eclipsed* conformation, Figure 3B, the hydroxyl groups at positions 2 and 3 of consecutive glucose units are optimally positioned to form hydrogen bonds, while they are at larger distance in other

https://doi.org/10.1021/acsomega.4c09367
ACS Omega 2025, 10, 4660−4669

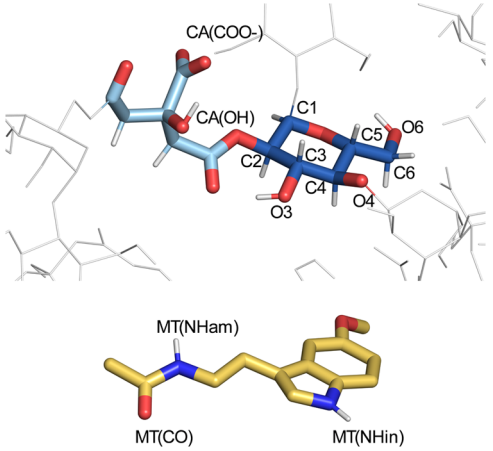

Figure 6. Atom labeling for the interactions shown in Tables S3 and S4 for nanosponges (top) and MT (bottom). Nonpolar hydrogen atoms of MT are omitted for clarity. MT: melatonin, CA: citric acid.

conformations. Therefore, by populating the canonical *eclipsed* conformation through MT binding, we observed an increased hydrogen bond frequency between the hydroxyl groups at positions 2 and 3 of consecutive glucose units compared to free β-CD. Figure 3B shows the distribution of hydrogen bond distances along the MD simulations of free β-CD and the MT:β-CD inclusion complex; while in the former less than one-fifth of the hydroxyl groups at positions 2 and 3 are forming hydrogen bonds, this fraction rises to about half in the latter.

We analyzed the geometric arrangement of the inclusion complex using a 2D representation based on two geometric descriptors: the radius of gyration (RoG) of MT, computed using its heavy atoms, and the distance between the center of mass of the six glycosidic oxygens (O4) of β-CD and the center of mass of MT, also computed using its heavy atoms. The coordinates of the initial structures in this two-dimensional representation are shown as red crosses (Figure 4A). We observed a densely populated region at low MT−β-CD distances (1−1.5 Å) and high MT RoGs (~3.4 to 3.5 Å). This is close to the *linear* geometry, which indicates that the MT remains extended and bound to β-CD through most of the simulation.

We performed geometric clustering to characterize with greater detail the conformations underlying the MT:β-CD inclusion complex arrangement. We identified two clusters that account for the 93% of the MD frames and correspond to two alternative conformations of a linear inclusion complex sharing the same MT RoG and MT−β-CD distance values. The representative geometries of these clusters are shown in Figure 4B. The most populated cluster, accounting for roughly two-thirds of the MD frames, is characterized by the insertion of MT with the indole moiety of MT close to C5 and C6 of α-glucose units. In the second cluster, accounting for roughly one-third of the frames, MT is inverted within the cavity with its indole group close to C3 and C5 of α-glucose units. Analysis of the noncovalent interactions on a selected MD frame representative of the first cluster (Figure S4) points to CH-π interactions between β-CD C(3)H and C(5)H (both fixed at axial positions) and C(6)H_2 (conformationally flexible) and the indole ring as the driving force for MT binding; this type of carbohydrate-aromatic interaction plays an important role in the recognition of saccharides by proteins.[46] Average distances for these contacts along the MD simulation of the inclusion complex are shown in Figure S5 and are shorter for C(5)H than for C(3)H and C(6)H as a consequence of the close contact of the MT indole group with C(5)H in both clusters. Finally, we computed the unbinding free energy using REUS simulations. The potential of mean force (PMF) is shown in Figure 4C. We found two additional shallow local minima, one at 0.6 kcal mol^{-1} from the global minimum, corresponding to the indole group buried in the β-CD cavity and the amide group exposed to the solvent, and a second one at 3.1 kcal mol^{-1} in which MT interacts with the outer surface of β-CD. The PMF tends to a dissociation energy of 3.8 kcal mol^{-1}. This value is in good agreement (within 0.2 kcal mol^{-1}) with the experimental K_b value of 871 M^{-1} (ΔG_b = −4.0 kcal mol^{-1}) determined spectroscopically at pH 7.[47] A previous work[48] based on calorimetric measurements indicates a K_b value of 48 M^{-1} (ΔG_b = −2.3 kcal mol^{-1}) at room temperature; overall, these values concur in describing a weak binding.

Nanosponges. We built nanosponge models with the cyclic and acyclic topologies shown in Figure 1B,1C, respectively. We ran MD simulations as four independent 500 ns replicas for each nanosponge model at maximum MT loading (1:1 MT:β-CD ratio). Loaded nanosponge geometries were initialized with each β-CD unit bound to a MT molecule in the *linear* conformation, which is the optimized inclusion complex geometry with closest resemblance to the arrange-

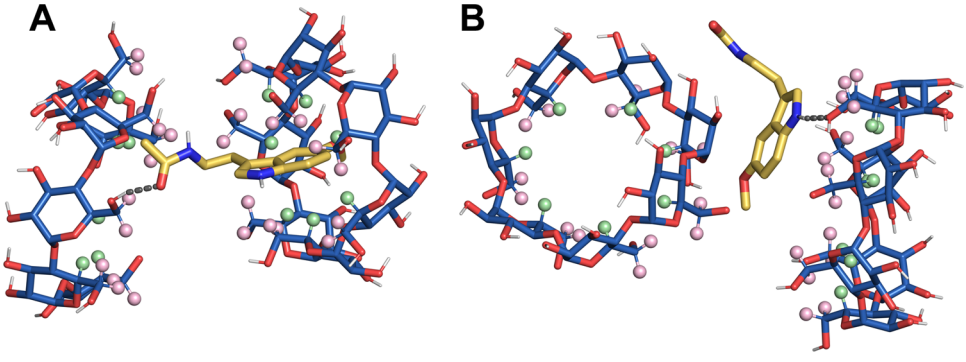

Figure 7. Examples of MT−nanosponges interactions from selected frames of the 7MT:β-CD-ns7c MD simulation characterizing alternative arrangements to the monomeric inclusion complex. (A) MT is only partially inserted in a β-CD cavity and forming a hydrogen bond with a second β-CD unit. (B) MT interacts with the external surface of two β-CD units. β-CD is shown as blue sticks, MT as yellow sticks, C5 hydrogens as green spheres and C6 hydrogens as pink spheres. Only the β-CD units involved in MT binding are shown for clarity.

https://doi.org/10.1021/acsomega.4c09367
ACS Omega 2025, 10, 4660−4669

ment observed in the previous MD simulations. We also performed MD for the same nanosponge models in the absence of MT to provide a reference in terms of unbound system flexibility.

Cross-linking has little effect on the intrinsic conformational freedom of β-CD units. The distributions of ϕ and ψ angles for both the loaded and free nanosponges are shown in Figures S6 and S7 and closely resemble those of the monomeric inclusion complex and free β-CD, respectively, with the only exception of a reduction in the *exo-syn-in* population for the two free nanosponges with cyclic topology (β-CD-ns5c and β-CD-ns7c, from 19 to 11−12%). As the *exo-syn-in* glycosidic bond conformation is incompatible with melatonin binding in the canonical inclusion complex arrangement due to steric hindrance, the depletion of *exo-syn-in* conformations in the free nanosponge models with cyclic topology compared with monomeric β-CD might contribute to the binding affinity of nanosponges through a larger average number of β-CD hydrophobic cavities available for binding. The higher rigidity of cyclic topologies is also reflected in lower RMSD values than their acyclic counterparts both when loaded with MT and in the free form (Table S1). The distribution of glucose ring conformations remains essentially unaffected, with the $^4C_1$ conformation representing over 92% of the population in all cases (Figures S8−S17).

We characterized MT-nanosponges interactions considering both the residence time of MT and specific noncovalent interactions responsible for binding. Table S2 shows how each MT unit is distributed along the MD simulations. "CD" labels refer to arrangements equivalent to the monomeric inclusion complex, identified by a MT−β-CD distance $\leq$3 Å. Frames corresponding to "unbound" situations are identified as those with both MT−β-CD distance >3 Å and MT Solvent Accessible Surface Area (SASA) $\geq$ 350 Å^2 (threshold value derived from MD simulations of free MT, Figure S19). The remaining frames correspond to alternative arrangements in which MT is bound to the nanosponges but not in a canonical inclusion complex arrangement. Owing to their intrinsic multivalency, nanosponges are expected to show a flexible binding profile. Indeed, unlike the monomeric inclusion complex in which MT remains buried at the CD cavity along most of the simulation, our nanosponge models show a dynamic binding behavior. In all cases, MTs evolve along different arrangements through the simulation leading to unbinding and alternative binding arrangements (noninclusion complexes). The high variability observed across both different nanosponge models and different MT molecules within the same model suggests that nanosponges create a wide variety of microenvironments that can lead to different binding interactions. Comparison of acyclic and cyclic topologies shows a similar average population of the canonical inclusion complex arrangement (54% of the simulation time for acyclic and 52% for cyclic topologies), and a higher population of alternative binding arrangement in cyclic topologies (40% of the simulation time vs only 30% in the acyclic ones). This is attributed to a higher stabilization of alternative binding arrangements in cyclic topologies owing to the formation of stable binding cavities defined by the outer surface of β-CD units and the cross-linker (*vide infra*, section Host−guest interactions).

In the largest model with cyclic topology, 7MT:β-CD-ns7c, we observe MT units switching positions by spontaneously unbinding from the CD unit to which they are initially complexed and associating to a different one. This is a direct observation of statistical rebinding, which is expected to endow nanosponges with an entropic advantage in terms of binding over monomeric β-CD (Figure 5). Statistical rebinding is a well-known mechanism to enhance multivalency in carbohydrate−protein recognition.[49] Figure 5A shows the evolution along the four MD replicas of the distances of three MT molecules (MT1, MT3, and MT6) from all the β-CD units of the 7MT:β-CD-ns7c system. While in replicas 1, 3, and 4 MTs remain bound to their original β-CD unit, in replica 2 they switch the local hosts in an exchange involving three MT molecules.

The process is described through selected MD frames in Figure 5B. The process is initiated by MT6 leaving the CD6 cavity and occupying a pocket defined by the external surfaces of CD3 and CD5. This is followed by the exchange of MT6 and MT1, and finally by MT3 binding into the empty cavity of CD6. As a further corroboration, we also performed MD simulations of the 1 MT:β-CD-ns7c complex, i.e., the same cyclic nanosponge topology with a single bound MT molecule. Again, we observed statistical rebinding with the MT molecule spontaneously hopping between two adjacent β-CD units (Figure S18 and Video S1), suggesting that this phenomenon is intrinsic to nanosponges binding at different loadings.

Host−Guest Interactions. We then proceeded to analyze the frequency of different types of contacts involved in MT binding. We considered all CH-π and hydrogen bond interactions between MT and the nanosponges, and classified the contacts according to the type of atoms involved in the interaction (Figure 6). The average number of contacts per atom type in the frames that present an inclusion-like arrangement are shown in Table S3.

CH-π interactions involving β-CD are the most frequent ones both in the monomeric complex and in the nanosponges, confirming that hydrophobic contacts are the leading enthalpic driving force for MT inclusion-like binding. While C(5)H dominates this type of interactions in the monomeric inclusion complex, in the nanosponges they are more evenly distributed among C(3)H, C(5)H, and C(6)H$_2$, suggesting a higher mobility of MT in the direction perpendicular to the β-CD ring. MT polar groups show increased hydrogen bond interactions with β-CD hydroxyl groups, which might pose an additional enthalpic benefit. We attribute this increase to the crowding induced by cross-linking, which raises the local concentration of hydrogen bond donors and acceptors in the proximity of bound MT molecules. Finally, we observe that interactions with the cross-linker are negligible, demonstrating that it is spatially separated from MT in the inclusion-like arrangement.

We characterized the distribution of the same interactions in the simulation frames classified as alternative MT binding arrangements (noninclusion) in the nanosponges (Table S4). In these noncanonical binding models we observe a reduction of the CH-π contacts involving β-CD C3 atoms, consistent with a displacement of MT molecules from the center of the cyclodextrin cavity, and an increase in CH-π interactions involving the more flexible hydroxymethyl group. Hydrogen bond interactions are redistributed between MT polar groups with an increase of those involving the NH group of the indole, which is less buried than at inclusion-like geometries. Two frames that exemplify these frequency shifts are shown in Figure 7A,7B. In the first one, MT is interacting preferentially with one β-CD unit but is only partially inserted, resembling

https://doi.org/10.1021/acsomega.4c09367
ACS Omega 2025, 10, 4660−4669

the second energy minimum in Figure 4C. This geometry is stabilized by a hydrogen bond involving the carbonyl of the amide and a glucopyranose hydroxymethyl group. In this type of geometry, CH-π interactions are still dominant since the hydrogens at C5 and C6 are available for binding. In the second frame, MT is simultaneously interacting with the external surfaces of two β-CD units, resembling the third energy minimum in Figure 4C. At this geometry, the indole ring can form both CH-π interactions and a hydrogen bond through its NH with glucopyranose hydroxymethyl groups. Interactions with the cross-linker are generally weak also in this arrangement and limited to hydrogen bonding with the free carboxylate. Overall, these results demonstrate that despite the higher availability of polar groups in noninclusion arrangements, the main driving force for MT binding is still van der Waals interactions.

CONCLUSIONS

We provide atomistic models of β-cyclodextrin monomer and related nanosponges cross-linked with citric acid with various topologies, and investigate their conformational landscape both in the free form and loaded with melatonin using molecular dynamics simulations. We classify the sampled binding arrangements characterizing the distribution of melatonin between inclusion and noninclusion binding poses. We demonstrate that despite differences in the local environments, the main driving force for melatonin binding is CH-π interactions between its indole group and β-CD units in all arrangements. We observe statistical rebinding and propose it as a mechanism for increased multivalency.

ASSOCIATED CONTENT

Data Availability Statement

The following data are available at 10.5281/zenodo.13839361 through the Zenodo repository (DOI: 10.5281/zenodo.13839360). Amber topologies, input coordinates and MD trajectories (PyMOL sessions) for the simulations of free MT in solution, free β-CD in solution, the monomeric MT:β-CD inclusion complex, all cyclic and acyclic nanosponge topologies both at maximum MT loading and in the free form.

Supporting Information

The Supporting Information is available free of charge at https://pubs.acs.org/doi/10.1021/acsomega.4c09367.

Computational methods for noncovalent interaction analysis. Distribution of ϕ and ψ values of the glycosidic bonds for free monomeric β-CD with different water force fields and maltose. Distribution of glucopyranose conformations (ring puckering) for free monomeric β-CD. Representation of noncovalent interactions in the MT:β-CD inclusion complex. Average CH-π distances for the monomeric MT:β-CD inclusion complex. Distribution of ϕ and ψ values of the glycosidic bonds of all nanosponge models. Distribution of glucopyranose conformations (ring puckering) for all nanosponge models. Solvent Accessible Surface Area for free melatonin. Spontanous unbinding and rebinding in the 1MT:β-CD-ns7c complex. Root mean square deviation values along the molecular dynamics simulations of all nanosponge models. Average MT contacts in the simulation of nanosponges corresponding to non-canonical binding arrangements. *cpptraj* script used for MD geometric clustering (PDF)

Video showing statistical rebinding in a nanosponge model with cyclic topology (ZIP)

AUTHOR INFORMATION

Corresponding Authors

Gonzalo Jiménez-Osés − *Center for Cooperative Research in Biosciences (CIC bioGUNE), Basque Research and Technology Alliance (BRTA) Bizkaia Technology Park, 48160 Derio, Spain; Ikerbasque, Basque Foundation for Science, 48013 Bilbao, Spain;* orcid.org/0000-0003-0105-4337; Email: gjoses@cicbiogune.es

Francesca Peccati − *Center for Cooperative Research in Biosciences (CIC bioGUNE), Basque Research and Technology Alliance (BRTA) Bizkaia Technology Park, 48160 Derio, Spain; Ikerbasque, Basque Foundation for Science, 48013 Bilbao, Spain;* orcid.org/0000-0002-7813-8216; Phone: +34 946 572 538; Email: fpeccati@cicbiogune.es

Authors

Riccardo Ferrero − *Dipartimento di Chimica and NIS Interdepartmental Centre, Università degli Studi di Torino, 10125 Torino, Italy*

Stefano Pantaleone − *Dipartimento di Chimica and NIS Interdepartmental Centre, Università degli Studi di Torino, 10125 Torino, Italy;* orcid.org/0000-0002-2457-1065

Valentina Brunella − *Dipartimento di Chimica and NIS Interdepartmental Centre, Università degli Studi di Torino, 10125 Torino, Italy*

Marta Corno − *Dipartimento di Chimica and NIS Interdepartmental Centre, Università degli Studi di Torino, 10125 Torino, Italy;* orcid.org/0000-0001-7248-2705

Complete contact information is available at: https://pubs.acs.org/10.1021/acsomega.4c09367

Notes

The authors declare no competing financial interest.

ACKNOWLEDGMENTS

This research has been funded by MCIN/AEI/10.13039/501100011033 (grants RYC2022-036457-I and EUR2023-143462 to F.P., PID2021-125946OB-I00 and PDC2022-133725-C22 to G.J.-O. and CEX2021-001136-S to CIC bioGUNE). S.P. and M.C. acknowledge European Union - Next Generation EU, Missione 4 Componente 1 CUP D13C22001340001 - CN00000013 and Spoke 7 "Materials and Molecular Sciences" of ICSC − Centro Nazionale di Ricerca in High-Performance Computing, Big Data and Quantum Computing, funded by the European Union − NextGenerationEU. R.F. is indebted to MUR for his PhD grant PON DM1061. R.F., S.P., V.B., and M.C. acknowledge support from Project CH4.0 under the MUR program "Dipartimenti di Eccellenza 2023−2027" (CUP: D13C22003520001).

REFERENCES

(1) Webber, M. J.; Langer, R. Drug delivery by supramolecular design. *Chem. Soc. Rev.* **2017**, *46*, 6600−6620.

(2) Braegelman, A. S.; Webber, M. J. Integrating Stimuli-Responsive Properties in Host-Guest Supramolecular Drug Delivery Systems. *Theranostics* **2019**, *9*, 3017−3040.

(3) Wenz, G. An Overview of Host-Guest Chemistry and its Application to Nonsteroidal Anti-Inflammatory Drugs. *Clin. Drug Investig.* **2000**, *19*, 21−25.
(4) Jacob, S.; Nair, A. B. Cyclodextrin complexes: Perspective from drug delivery and formulation. *Drug Dev. Res.* **2018**, *79*, 201−217.
(5) Wankar, J.; Kotla, N. G.; Gera, S.; Rasala, S.; Pandit, A.; Rochev, Y. A. Recent Advances in Host−Guest Self-Assembled Cyclodextrin Carriers: Implications for Responsive Drug Delivery and Biomedical Engineering. *Adv. Funct. Mater.* **2020**, *30*, No. 1909049.
(6) Suárez, D.; Díaz, N. Conformational and entropy analyses of extended molecular dynamics simulations of α-, β- and γ-cyclodextrins and of the β-cyclodextrin/nabumetone complex. *Phys. Chem. Chem. Phys.* **2017**, *19*, 1431−1440.
(7) Thaning, J.; Stevensson, B.; Östervall, J.; Naidoo, K. J.; Widmalm, G.; Maliniak, A. NMR Studies of Molecular Conformations in α-Cyclodextrin. *J. Phys. Chem. B* **2008**, *112*, 8434−8436.
(8) Gebhardt, J.; Kleist, C.; Jakobtorweihen, S.; Hansen, N. Validation and Comparison of Force Fields for Native Cyclodextrins in Aqueous Solution. *J. Phys. Chem. B* **2018**, *122*, 1608−1626.
(9) Sherje, A. P.; Dravyakar, B. R.; Kadam, D.; Jadhav, M. Cyclodextrin-based nanosponges: A critical review. *Carbohydr. Polym.* **2017**, *173*, 37−49.
(10) Xie, Z.; Chen, F.; Li, W. A.; Geng, X.; Li, C.; Meng, X.; Feng, Y.; Liu, W.; Yu, F. A review of sleep disorders and melatonin. *Neurol. Res.* **2017**, *39*, 559−565.
(11) Kostoglou-Athanassiou, I. Therapeutic applications of melatonin. *Therapeutic Adv. Endocrinol. Metabolism* **2013**, *4*, 13−24.
(12) Sakellaropoulou, A.; Siamidi, A.; Vlachou, M. Melatonin/Cyclodextrin Inclusion Complexes: A Review. *Molecules* **2022**, *27*, 445.
(13) Pantaleone, S.; Gho, C. I.; Ferrero, R.; Brunella, V.; Corno, M. Exploration of the Conformational Scenario for α-, β-, and γ-Cyclodextrins in Dry and Wet Conditions, from Monomers to Crystal Structures: A Quantum-Mechanical Study. *Int. J. Mol. Sci.* **2023**, *24*, No. 16826.
(14) Ferrero, R.; Pantaleone, S.; Delle Piane, M.; Caldera, F.; Corno, M.; Trotta, F.; Brunella, V. On the Interactions of Melatonin/β-Cyclodextrin Inclusion Complex: A Novel Approach Combining Efficient Semiempirical Extended Tight-Binding (xTB) Results with Ab Initio Methods. *Molecules* **2021**, *26*, 5881.
(15) Pyrak, B.; Rogacka-Pyrak, K.; Gubica, T.; Gubica, Ł. Exploring Cyclodextrin-Based Nanosponges as Drug Delivery Systems: Understanding the Physicochemical Factors Influencing Drug Loading and Release Kinetics. *Int. J. Mol. Sci.* **2024**, *25*, 3527.
(16) Tiwari, K.; Bhattacharya, S. The ascension of nanosponges as a drug delivery carrier: preparation, characterization, and applications. *J. Mater. Sci.: Mater. Med.* **2022**, *33*, 28.
(17) Garg, A.; Lai, W.-C.; Chopra, H.; Agrawal, R.; Singh, T.; Chaudhary, R.; Dubey, B. N. Nanosponge: A promising and intriguing strategy in medical and pharmaceutical Science. *Heliyon* **2024**, *10*, No. e23303.
(18) Sharma, S.; Parveen, R.; Chatterji, B. P. Toxicology of Nanoparticles in Drug Delivery. *Curr. Pathobiol. Rep.* **2021**, *9*, 133−144.
(19) Trotta, F.; Cavalli, R. Characterization and applications of new hyper-cross-linked cyclodextrins. *Compos. Interfaces* **2009**, *16*, 39−48.
(20) Raffaini, G.; Ganazzoli, F.; Mele, A.; Castiglione, F. A molecular dynamics study of cyclodextrin nanosponge models. *J. Incl. Phenom. Macrocycl. Chem.* **2013**, *75*, 263−268.
(21) Wang, H.; Yapa, A. S.; Kariyawasam, N. L.; et al. Rationally designed peptide nanosponges for cell-based cancer therapy. *Nanomed.: Nanotechnol. Biol. Med.* **2017**, *13*, 2555−2564.
(22) Suvarna, V.; Singh, V.; Sharma, D.; Murahari, M. Experimental and computational insight of the supramolecular complexes of Irbesartan with β-cyclodextrin based nanosponges. *J. Drug Delivery Sci. Technol.* **2021**, *63*, No. 102494.
(23) Pedrazzo, A. R.; Smarra, A.; Caldera, F.; Musso, G.; Dhakar, N. K.; Cecone, C.; Hamedi, A.; Corsi, I.; Trotta, F. Eco-Friendly β-cyclodextrin and Linecaps Polymers for the Removal of Heavy Metals. *Polymers* **2019**, 1−14.
(24) Krabicová, I.; Appleton, S. L.; Tannous, M.; Hoti, G.; Caldera, F.; Rubin Pedrazzo, A.; Cecone, C.; Cavalli, R.; Trotta, F. History of Cyclodextrin Nanosponges. *Polymers* **2020**, *12*, 1122.
(25) Hoti, G.; Ferrero, R.; Caldera, F.; Trotta, F.; Corno, M.; Pantaleone, S.; Desoky, M. M.; Brunella, V. A Comparison between the Molecularly Imprinted and Non-Molecularly Imprinted Cyclodextrin-Based Nanosponges for the Transdermal Delivery of Melatonin. *Polymers* **2023**, *15*, 1543.
(26) Case, D.et al. *AMBER 2022*, 2023.
(27) Kirschner, K. N.; Yongye, A. B.; Tschampel, S. M.; González-Outeiriño, J.; Daniels, C. R.; Foley, B. L.; Woods, R. J. GLYCAM06: A generalizable biomolecular force field Carbohydrates. *J. Comput. Chem.* **2008**, *29*, 622−655.
(28) He, X.; Man, V. H.; Yang, W.; Lee, T.-S.; Wang, J. A fast and high-quality charge model for the next generation general AMBER force field. *J. Chem. Phys.* **2020**, *153*, No. 114502.
(29) Izadi, S.; Onufriev, A. V. Accuracy limit of rigid 3-point water models. *J. Chem. Phys.* **2016**, *145*, No. 074501.
(30) Izadi, S.; Anandakrishnan, R.; Onufriev, A. V. Building Water Models: A Different Approach. *J. Phys. Chem. Lett.* **2014**, *5*, 3863−3871.
(31) Jorgensen, W. L.; Chandrasekhar, J.; Madura, J. D.; Impey, R. W.; Klein, M. L. Comparison of simple potential functions for simulating liquid water. *J. Chem. Phys.* **1983**, *79*, 926−935.
(32) Sengupta, A.; Li, Z.; Song, L. F.; Li, P.; Merz, K. M. J. Parameterization of Monovalent Ions for the OPC3, OPC, TIP3P-FB, and TIP4P-FB Water Models. *J. Chem. Inf. Model.* **2021**, *61*, 869−880.
(33) (a) Andersen, H. C. Molecular dynamics simulations at constant pressure and/or temperature. *J. Chem. Phys.* **1980**, *72*, 2384−2393. (b) Andrea, T. A.; Swope, W. C.; Andersen, H. C. The role of long ranged forces in determining the structure and properties of liquid water. *J. Chem. Phys.* **1983**, *79*, 4576−4584.
(34) Miyamoto, S.; Kollman, P. A. Settle: An analytical version of the SHAKE and RATTLE algorithm for rigid water models. *J. Comput. Chem.* **1992**, *13*, 952−962.
(35) Darden, T.; York, D.; Pedersen, L. Particle mesh Ewald: An Nlog(N) method for Ewald sums in large systems. *J. Chem. Phys.* **1993**, *98*, 10089−10092.
(36) Roe, D. R.; Cheatham, T. E. I. PTRAJ and CPPTRAJ: Software for Processing and Analysis of Molecular Dynamics Trajectory Data. *J. Chem. Theory Comput.* **2013**, *9*, 3084−3095.
(37) Sabri Dashti, D.; Roitberg, A. E. Optimization of Umbrella Sampling Replica Exchange Molecular Dynamics by Replica Positioning. *J. Chem. Theory Comput.* **2013**, *9*, 4692−4699.
(38) Loncharich, R. J.; Brooks, B. R.; Pastor, R. W. Langevin dynamics of peptides: The frictional dependence of isomerization rates of N-acetylalanyl-N'-methylamide. *Biopolymers* **1992**, *32*, 523−535.
(39) Grossfield, A. *WHAM: The Weighted Histogram Analysis Method, Version 2.0.11*.
(40) Kozár, T.; Venanzi, C. A. Reconsidering the conformational flexibility of β-cyclodextrin. *J. Mol. Struct. THEOCHEM* **1997**, *395*−*396*, 451−468.
(41) Khuntawee, W.; Karttunen, M.; Wong-ekkabut, J. A molecular dynamics study of conformations of beta-cyclodextrin and its eight derivatives in four different solvents. *Phys. Chem. Chem. Phys.* **2017**, *19*, 24219−24229.
(42) Cézard, C.; Trivelli, X.; Aubry, F.; Djedaïni-Pilard, F.; Dupradeau, F.-Y. Molecular dynamics studies of native and substituted cyclodextrins in different media: 1. Charge derivation and force field performances. *Phys. Chem. Chem. Phys.* **2011**, *13*, 15103−15121.
(43) Quevedo, M. A.; Zoppi, A. Current trends in molecular modeling methods applied to the study of cyclodextrin complexes. *J. Incl. Phenom. Macrocycl. Chem.* **2018**, *90*, 1−14.
(44) Sattelle, B. M.; Almond, A. Less is more when simulating unsulfated glycosaminoglycan 3D-structure: Comparison of GLY-

https://doi.org/10.1021/acsomega.4c09367
ACS Omega 2025, 10, 4660−4669

CAM06/TIP3P, PM3-CARB1/TIP3P, and SCC-DFTB-D/TIP3P predictions with experiment. *J. Comput. Chem.* **2010**, *31*, 2932−2947.
(45) Mostad, A.; Rømming, C.; et al. The Crystal and Molecular Structure of N-Acetyl-5-methoxy-tryptamine (Melatonin). *Acta Chem. Scand.* **1974**, *28b*, 564−572.
(46) Asensio, J. L.; Ardá, A.; Cañada, F. J.; Jiménez-Barbero, J. Carbohydrate−Aromatic Interactions. *Acc. Chem. Res.* **2013**, *46*, 946−954.
(47) Zafra-Roldán, A.; Corona-Avendaño, S.; Montes-Sánchez, R.; Palomar-Pardavé, M.; Romero-Romo, M.; Ramírez-Silva, M. New insights on the spectrophotometric determination of melatonin pKa values and melatonin-βCD inclusion complex formation constant. *Spectrochim. Acta A Mol. Biomol. Spectrosc.* **2018**, *190*, 442−449.
(48) Bongiorno, D.; Ceraulo, L.; Mele, A.; Panzeri, W.; Selva, A.; Turco Liveri, V. Structural and physicochemical characterization of the inclusion complexes of cyclomaltooligosaccharides (cyclodextrins) with melatonin. *Carbohydr. Res.* **2002**, *337*, 743−754.
(49) van Heteren, J.; Pieters, R. J. *Carbohydrates in Drug Discovery and Development*; Tiwari, V. K., Ed.; Elsevier, 2020; pp 383−402.

https://doi.org/10.1021/acsomega.4c09367
ACS Omega 2025, 10, 4660−4669